Accepted Manuscript online: 2022-04-25 Article published online: 2022-05-10

Donor–Acceptor Copolymers with Rationally Regulated Side Chain Orientation for Polymer Solar Cells Processed by Non-Halogenated Solvent

Zhengwei Hu[#a]
Qiri Huang[#a]
Chunchen Liu[*a]
Ao Song[a]
Lin Shao[a]
Yuanqing Bai[a]
Zhicheng Hu[a]
Kai Zhang[a]
Fei Huang[*a]
Yong Cao[a]

[a] Institute of Polymer Optoelectronic Materials and Devices, State Key Laboratory of Luminescent Materials and Devices, South China University of Technology, Guangzhou, 510640 (P. R. of China)
[#] Equally contributed.
[*] msfhuang@scut.edu.cn; mscliu@scut.edu.cn

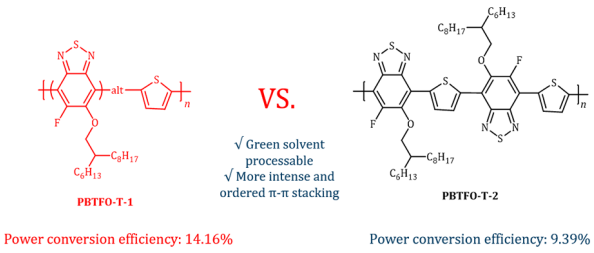

Received: 11.02.2022
Accepted after revision: 05.04.2022
DOI: 10.1055/a-1833-8668; Art ID: OM-2022-02-0002-OA

Abstract A donor–acceptor (D-A) conjugated polymer PBTFO-T-1 consisting of 2,1,3-benzothiadiazole (BT) as A unit and thiophene (T) as D unit was facilely obtained by a straightforward three-step reaction. The BT unit is attached with a fluorine atom and an alkoxy chain to simultaneously endow the polymer with a deep HOMO energy level and desirable solubility. The alkoxyl chain orientation on the BT unit has been regulated and the polymer PBTFO-T-2 with regio-regularly oriented side chains was also developed to investigate the impact of the alkoxyl chain orientation on their optoelectronic properties. The PBTFO-T-1:Y6-BO polymer solar cells (PSCs) were processed with a non-halogenated solvent and achieved an optimized power conversion efficiency of 14.16%, significantly higher than 9.39% of the PBTFO-T-2:Y6-BO counterpart. It has been demonstrated that the PBTFO-T-1:Y6-BO film exhibits higher and more balanced charge transportation and superior film morphology, resulting in higher exciton generation and dissociation, less recombination and eventually the higher short-circuit current density (J_{SC}) and fill factor. This study provides a possible strategy to develop polymer donors with low cost for future commercial applications of PSCs and gives some insights into regulating optoelectronic properties of polymer donors via rationally modifying their side chain orientation.

Key words: polymer donor, non-halogenated solvent, regio-regular orientation

Introduction

Polymer solar cells (PSCs) have attracted extensive research attention and achieved rapid development in recent years due to their advantages of light weight, flexibility and feasibility of roll-to-roll process.[1–6] Active layer materials with bulk heterojunction (BHJ) structure formed by mechanical blending are important components of PSCs, which are usually composed of p-type polymer electron donors and n-type small molecule or polymer electron acceptors.[7–9] In the past few years, the power conversion efficiency (PCE) of PSCs has been boosted from 10% to over 18% because of the rapid development of various non-fullerene small molecular acceptors (NFSMAs) and polymer donors.[10–15] Recently, numerous efforts of researchers have been mainly devoted to the design of novel NFSMAs or delicate molecular modification on developed NFSMAs to continuously improve PCE.[16–24] Meanwhile, polymer donors with the complementary absorption spectra, matched energy levels and promising charge transporting abilities also play a synergic and vital role in promoting the PCE, which thus should be paid considerable attention for accelerating the commercial application of PSCs.[25–33]

Considering that the PSC technology has come to a crossroad towards commercial application, the cost must be taken into account when developing active layer materials.[34] The cost mainly comes from the tedious synthesis works, low yield and the usage of expensive starting materials for preparing donor and acceptor materials.[35] However, to the best of our knowledge, the research studies on decreasing the cost of polymer donors lag far behind the exploration on various high-efficiency polymer donors. A majority of

high-efficiency polymer donors are prohibitively expensive for commercial applications due to their complex molecular structures, cumbersome synthesis, and complicated purification process.[36–38] To date, only a few polymer donors have been reported to simultaneously possess the merits of low cost and high PCE. The typical representatives are high-efficiency polythiophene derivatives, poly[(thiophene)-*alt*-(6,7-difluoro-2-(2-hexyldecyloxy)quinoxaline)] (PTQ10), etc.[39–46] Additionally, processing the PSCs with non-halogenated/green solvents is another essential prerequisite for their commercial applications.[47–52] Therefore, it is of vital significance to construct cost-effective, high-performance and green solvent processable polymer donors with low-cost starting compounds and shorted synthesis steps.

Herein, a low-cost polymer donor, poly[(thiophene)-*alt*-(5-fluoro-6-((2-hexyldecyl)oxy)benzo[*c*][1,2,5]thiadiazole)] (PBTFO-T-1), was designed and synthesized with high yield through a simple and straightforward three-step reaction. The polymer PBTFO-T-1 backbone is constructed with alternating benzothiadiazole (BT) as the acceptor moiety and thiophene (T) as the donor moiety, both of which are commonly used units in organic optoelectronic materials and are available in large scale at low cost. Fluorine atom and alkoxyl chain attachments are employed on the BT unit to endow the designed polymers with lower HOMO energy level, stronger π–π stacking and requirable solubilty.[53] Another polymer PBTFO-T-2 with regio-regularly oriented alkoxyl chains is also prepared to investigate the effect of alkoxyl chain orientation on PSCs' performance. The PSCs based on PBTFO-T-1:Y6-BO achieved an optimal PCE of 14.16% through processing with a non-halogenated solvent, o-xylene, significantly higher than 9.39% of PBTFO-T-2:Y6-BO counterparts. It is found that PBTFO-T-1 with a lower cost exhibits more intense and ordered π–π aggregation than PBTFO-T-2, and the higher short-circuit current density (J_{sc}) and fill factor (FF) of PBTFO-T-1:Y6-BO can be ascribed to the more balanced charge transportation, lower charge recombination, higher exciton generation and dissociation, and better blend film morphology.

Results and Discussion

Copolymers PBTFO-T-1 and PBTFO-T-2 were synthesized by Stille copolymerization of 2,5-bis(trimethylstannyl)thiophene with key monomers 4,7-dibromo-5-fluoro-6-((2-hexyldecyl)oxy)benzo[*c*][1,2,5]thiadiazole (**M1**) and 2,5-bis(7-bromo-6-fluoro-5-((2-hexyldecyl)oxy)benzo[*c*][1,2,5]thiadiazol-4-yl)thiophene (**M2**), respectively (Scheme 1). Detailed synthesis procedures and characterization of the intermediates and polymers are described in the Experimental Section and Supporting Information. PBTFO-T-1 can be facilely obtained by the straightforward three-step reaction, which is commenced with di-bromination of commercially available difluorobenzo[*c*][1,2,5]thiadiazole (**1**) to afford 4,7-dibromo-5,6-difluorobenzo[*c*][1,2,5]thiadiazole (**2**) with a yield of 60%. Subsequently, compound **2** was mono-substituted with an alkoxyl chain to afford the key intermediate **M1** in 72% yield, which was followed by palladium-catalyzed Stille polymerization with commercially available 2,5-bis(trimethylstannyl)thiophene to afford the final polymer PBTFO-T-1 in ~80% yield. For PBTFO-T-2 with regio-regularly arranged alkoxyl chains, two more steps were required to synthesize the key intermediate **M2**. Commercially available compound **1** was firstly transformed to mono-alkoxyl chain-substituted 5-fluoro-6-((2-hexyldecyl)oxy)benzo[*c*][1,2,5]thiadiazole (**3**) in 80% yield, which was followed by selective mono-bromination under bromine to afford 4-bromo-6-fluoro-5-((2-hexyldecyl)oxy)benzo[*c*][1,2,5]thiadiazole (**4**) in a yield of 88%. Then the intermediate **M2** was prepared via one step of Stille coupling reaction with 2,5-bis(trimethylstannyl)thiophene and a straightforward step of di-bromination reaction. Finally, PBTFO-T-2 was obtained via the same polymerization procedures with PBTFO-T-1. These synthesis details suggested that the preparation of PBTFO-T-1 was more cost-effective than that of PBTFO-T-2.

The obtained PBTFO-T-1 and PBTFO-T-2 are well soluble in chloroform, o-xylene and other common processing solvents. The number-average molecular weights (M_n)/polydispersity index (PDI) were measured to be 38.0 kDa/2.24 and 34.6 kDa/1.98 for PBTFO-T-1 and PBTFO-T-2, respectively (Figure S16). The thermal properties of PBTFO-T-1 and PBTFO-T-2 were evaluated by thermogravimetric analysis (TGA) and differential scanning calorimetry (DSC) (Figure S13). The 5% weight-loss temperatures of PBTFO-T-1 and PBTFO-T-2 are 339 °C and 344 °C, respectively, indicating that both polymers have good thermal stability. The DSC results show no phase transition peaks for PBTFO-T-1 and PBTFO-T-2, suggesting their amorphous features.

The UV-vis absorption spectra of PBTFO-T-1 and PBTFO-T-2 in chloroform solutions and as films and Y6-BO film are shown in Figure 1b. This reveals that the absorption spectra of PBTFO-T-1 and PBTFO-T-2 in solvents and films are similar and mainly range from 500 to 700 nm, which can form complementary absorption for Y6-BO with the main absorption region ranging from 600 to 900 nm. The $\lambda_{onset(film)}$ values of PBTFO-T-1 and PBTFO-T-2 were estimated to be 742 and 738 nm, respectively. The absorption shapes of the two polymers were scrutinized and a distinct difference could be figured out. The shoulder absorption at ~671 nm of PBTFO-T-1 was apparently stronger than that of PBTFO-T-2 in film, suggesting more intense and ordered π–π stacking of PBTFO-T-1 in film. This indicates that the orientation of fluorine atoms and alkoxy chains has a very significant influence on the packing of polymer molecules. In order to confirm this conjecture, temperature-dependent absorption spectrum measurements were conducted to in-

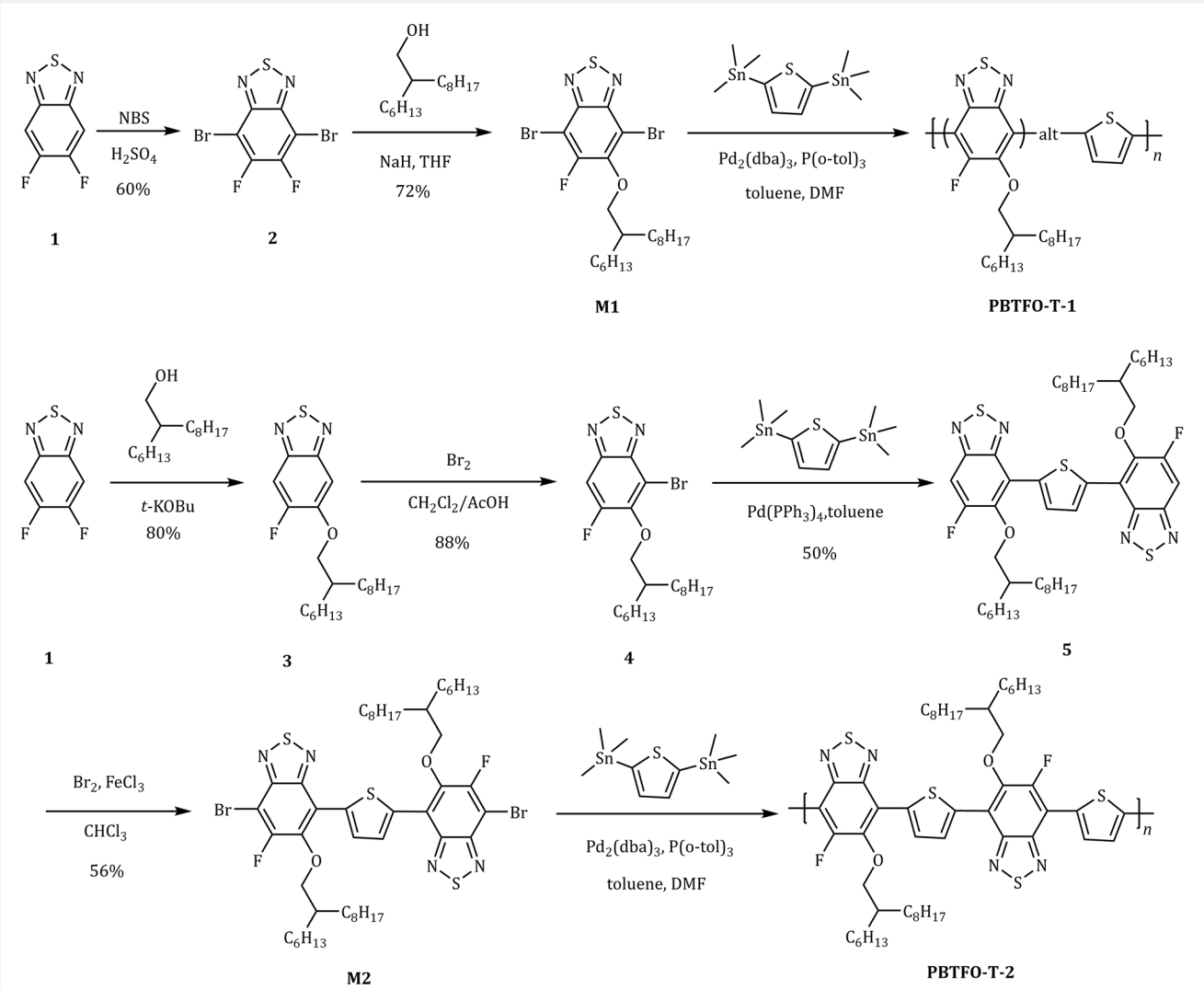

Scheme 1 The synthetic routes for PBTFO-T-1 and PBTFO-T-2.

vestigate the aggregation properties of the polymers in dilute chlorobenzene solutions (Figure S14). The 0–0 transition peaks indicated that the aggregation behaviors of PBTFO-T-1 and PBTFO-T-2 were both gradually weakened as the temperature increased. Notably, when PBTFO-T-2 was heated to 65 °C, its 0–0 transition peak disappeared completely, while the 0–0 transition peak of PBTFO-T-1 could still be observed even at 95 °C. This confirms that PBTFO-T-1 has a stronger aggregation behavior. By carefully comparing the absorption of the two polymers in films and solutions, a ~ 11 nm red-shift can be observed for the PBTFO-T-1 film while the red-shift of PBTFO-T-2 is almost absent, further suggesting the weaker aggregation of PBTFO-T-2. The combined phenomena demonstrate that PBTFO-T-1 with randomly oriented alkoxyl chains exhibits stronger aggregation than PBTFO-T-2 with regio-regularly oriented alkoxyl chains.

The HOMO energy levels of PBTFO-T-1 and PBTFO-T-2 were estimated by initial oxidation potentials (∂_{ox}) obtained from cyclic voltammetry (Figure S15) according to the formula: HOMO = $-e(\partial_{ox} + 4.8 - \partial_{Fc/Fc+})$. Ferrocene/ferrocenium ($\partial_{Fc/Fc+}$) was used as a reference with an oxidation potential of 0.39 V. The ∂_{ox} values of PBTFO-T-1 and PBTFO-T-2 are 1.09 and 1.15 V, respectively, and their corresponding HOMO energy levels are − 5.50 and − 5.56 eV, respectively. The LUMO energy levels of PBTFO-T-1 and PBTFO-T-2 were calculated to be − 3.83 and − 3.88 eV, respectively, based on their HOMO energy levels and optical band gaps (E_g^{opt}) according to the formulas: $E_g^{opt} = 1240/\lambda_{onset(film)}$ and LUMO = HOMO + E_g^{opt}. The HOMO and LUMO energy levels of Y6-BO

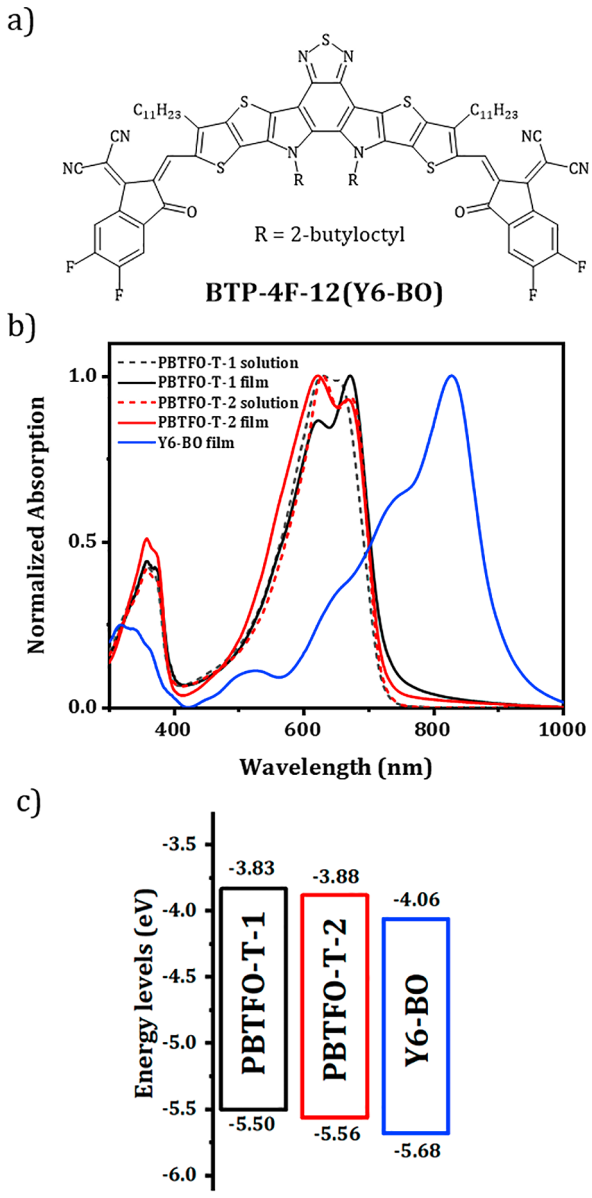

Figure 1 a) Molecular structure of Y6-BO. b) The normalized UV-vis absorption of two polymer donors and Y6-BO, and c) their energy level diagrams.

(Figure 1a) reported in the literature[54] were compared with the measured results of these two polymers (Figure 1c). The result demonstrates that the energy levels are matched and the driving force for charge separation is sufficient when these polymers are used as a donor and Y6-BO is used as an acceptor in PSCs.

To study the effect of alkoxyl chain orientation on photovoltaic performance, BHJ-PSC devices with PBTFO-T-1 and

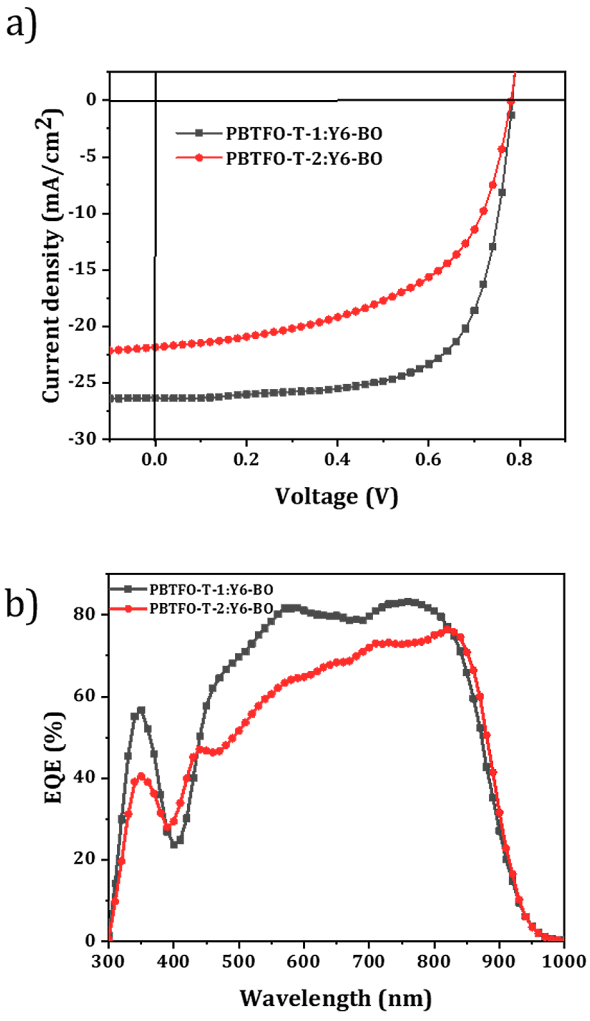

Figure 2 a) *J–V* curves and b) EQE spectrum of PBTFO-T-1- and PBTFO-T-2-based devices.

PBTFO-T-2 as donors were fabricated and examined under AM1.5 G solar illumination (100 mW·cm^{-2}). The devices were fabricated with a conventional architecture of ITO/PEDOT:PSS/polymer donor:non-fullerene small-molecule acceptor/PNDIT-F3 N (NDI)/Ag. The detailed device optimization process is presented in the Supporting Information (Figures S18–S23). The current density–voltage (*J–V*) curves and external quantum efficiency (EQE) spectra are shown in Figure 2a and 2b, and all performance parameters are presented in Table 1. The optimal PBTFO-T-1-based devices can obtain a PCE of 14.16% with an open-circuit voltage (V_{OC}) of 0.80 V, a short-circuit current density (J_{SC}) of 25.34 mA·cm^{-2} and a FF of 70.99%. However, the optimal PBTFO-T-2-based devices can only achieve a PCE of 9.39% with a V_{OC} of 0.78 V, a J_{SC} of 21.85 mA·cm^{-2} and a FF of

Table 1 The photovoltaic parameters of the optimal devices

Active layer[a]	V_{OC} (V)	J_{SC} (mA·cm^{-2})	$J_{SC(EQE)}$ (mA·cm^{-2})[b]	FF (%)	PCE_{max} (%)
PBTFO-T-1:Y6-BO	0.80	25.34 (25.30 ± 0.03)	24.22	70.99 (70.25 ± 0.57)	14.16
PBTFO-T-2:Y6-BO	0.78	21.85 (21.74 ± 0.10)	21.29	55.55 (54.45 ± 1.51)	9.39

[a]The devices were fabricated with an architecture of ITO/PEDOT:PSS/polymer donor:Y6-BO/PNDIT-F3 N (NDI)/Ag. The ratio of the donor:acceptor was 1:1.2. O-xylene as the processing solvent.
[b]Calculated from the integration of EQE spectra.

55.55%. During the optimization of the devices, we can find that a higher PCE can be obtained when Y6-BO is used as the acceptor compared with other acceptors. Particularly, we are pleased to find that PBTFO-T-1:Y6-BO and PBTFO-T-2:Y6-BO devices can achieve higher PCEs when o-xylene is used as the processing solvent. O-xylene is a non-halogenated solvent and more environment-friendly than halogenated solvents, which will be very beneficial for commercial application of PSCs. Although PBTFO-T-2 has a deeper HOMO level than PBTFO-T-1, the V_{OC} values of the PBTFO-T-1-based devices are larger than those of the PBTFO-T-2-based devices, which may be due to the larger non-radiative loss of the PBTFO-T-2-based devices.[55] The J_{SC} values calculated from EQE are 24.22 and 21.29 mA·cm^{-2} for PBTFO-T-1- and PBTFO-T-2-based devices, respectively, both of which are within a 5% error region, demonstrating the reliability of the obtained data. The higher FF of the PBTFO-T-1-based devices is presumably ascribed to their better charge transport in the active layer and less charge recombination, which will be investigated later.

The curves of photocurrent density (J_{ph}) versus effective voltage (V_{eff}) of the devices are shown in Figure 3a, which are commonly used to investigate exciton generation.[56] Typically, in the saturation photocurrent (J_{sat}) region, all excitons dissociate into free charge carriers and are collected by the electrodes. As shown in Figure 3a, the J_{sat} of the PBTFO-T-1-based device is 26.62 mA·cm^{-2}, higher than 21.99 mA·cm^{-2} of the PBTFO-T-2-based device. The maximum photocarrier generation rate (G_{max}) can be determined from the number of absorbed photons, which can also be calculated by the equation: $G_{max} = J_{sat}/qd$, where q is the electron charge and d is the thickness of the active layer.[57] By calculation, the G_{max} values of 1.51×10^{27} and 1.21×10^{27} m^3·s^{-1} are gained for PBTFO-T-1- and PBTFO-T-2-based devices, respectively, indicating a faster exciton generation rate of the PBTFO-T-1-based device. The charge collection probability $P(E, T)$, which is the function of the electric field (E) and temperature (T), was estimated using the equation: $P(E, T) = J_{ph}/J_{sat}$.[58] Under short-circuit conditions, the $P(E, T)$ values of 95.2% and 90.47% were calculated for PBTFO-T-1- and PBTFO-T-2-based devices, respectively, demonstrating the higher exciton dissociation efficiency of the PBTFO-T-1-based device. These results well explain the underlying mechanism of the higher J_{SC} and FF of the PBTFO-T-1-based devices.

We characterized the charge transport properties of the pure polymer films and blended active-layer films based on the space-charge-limited current (SCLC) mobility method.[59] The J–V curves of the hole-only and electron-only devices are shown in the Supporting Information (Figure S17) and

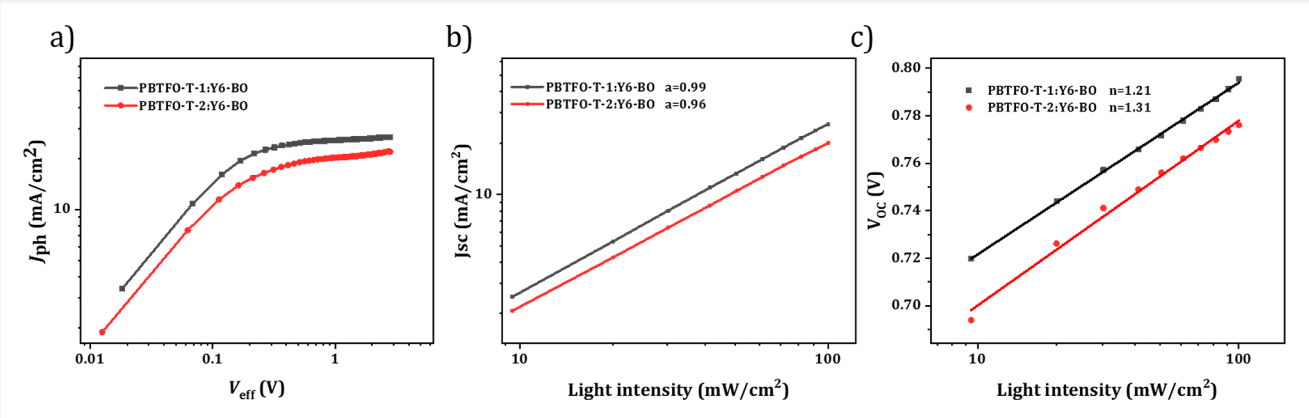

Figure 3 a) Curves of J_{ph} versus V_{eff} for PBTFO-T-1- and PBTFO-T-2-based devices. b) Light intensity dependence of J_{SC} of PBTFO-T-1- and PBTFO-T-2-based devices. c) Light intensity dependence of V_{OC} of PBTFO-T-1- and PBTFO-T-2-based devices.

Table 2 The carrier mobilities of pure polymer films and blended active-layer films[a]

	μ_h ($cm^2 \cdot V^{-1} \cdot s^{-1}$)	μ_e ($cm^2 \cdot V^{-1} \cdot s^{-1}$)	$\mu_h\mu_e$
PBTFO-T-1	5.52×10^{-4}	NA	NA
PBTFO-T-2	2.88×10^{-4}	NA	NA
PBTFO-T-1:Y6-BO	4.75×10^{-3}	1.49×10^{-3}	1.74
PBTFO-T-2:Y6-BO	2.58×10^{-3}	1.20×10^{-3}	3.97

[a] Mobility data were measured by the SCLC method. NA: not available.

the hole/electron mobility data are summarized in Table 2. The hole mobility of the PBTFO-T-1 film is 5.52×10^{-4} $cm^2 \cdot V^{-1} \cdot s^{-1}$, 1.92 times higher over 2.88×10^{-4} $cm^2 \cdot V^{-1} \cdot s^{-1}$ of the PBTFO-T-2 film. After blending with Y6-BO, the PBTFO-T-1:Y6-BO blended film exhibits a hole mobility of 4.75×10^{-3} $cm^2 \cdot V^{-1} \cdot s^{-1}$ and an electron mobility of 1.49×10^{-3} $cm^2 \cdot V^{-1} \cdot s^{-1}$, while the PBTFO-T-2:Y6-BO-based devices display a lower hole mobility of 2.58×10^{-3} $cm^2 \cdot V^{-1} \cdot s^{-1}$ and an electron mobility of 1.20×10^{-3} $cm^2 \cdot V^{-1} \cdot s^{-1}$. Additionally, the PBTFO-T-1:Y6-BO-based device displays a more balanced charge transport behavior ($\mu_h\mu_e = 1.74$) compared to that of PBTFO-T-2:Y6-BO-based device ($\mu_h\mu_e = 3.97$). The higher and more balanced charge mobility can improve the charge transport properties of photovoltaic devices, as evidenced by the significantly enhanced FF and J_{SC} of the PBTFO-T-1:Y6-BO-based devices.

The dependence of J_{SC} and V_{OC} on light intensity was further examined to analyze the recombination behavior of carriers.[60] As shown in Figure 3b and 3c, the relationship between J_{SC} and P_{light} can be expressed as $J_{SC} \propto P_{light}^{S}$, where P_{light} is the light intensity and S is the exponential factor. The S values of the PBTFO-T-1- and PBTFO-T-2-based devices were calculated to be 0.99 (closer to 1) and 0.96, respectively. This indicates that there is less bimolecular recombination in the PBTFO-T-1:Y6-BO-based devices, resulting in the higher FF of the PBTFO-T-1:Y6-BO-based devices. Plotting V_{OC} as a function of the natural logarithm of P_{light}, we obtained the slope nkT/q, where $n = 1$ or 2 represents predominant biomolecular recombination or trap-assisted single-molecule recombination, respectively.[61] The slope of 1.21 kT/q and 1.31 kT/q can be calculated for PBTFO-T-1:Y6-BO- and PBTFO-T-2:Y6-BO-based devices, respectively, indicating that the PBTFO-T-1:Y6-BO-based device has a lower trap-assisted monomolecular recombination.

We further use atomic force microscopy (AFM) to investigate the effect of alkoxyl chain orientation on polymer films and polymer:Y6-BO active-layer film morphology (Figure 4). The root-mean-square roughness (R_q) of PBTFO-T-1 and PBTFO-T-2 pristine films was 2.60 and 1.88 nm, respectively. The surface of PBTFO-T-1 is rougher and exhibits a stronger aggregation behavior as confirmed by the aforementioned measurements. For polymer:Y6-BO blended films, the PBTFO-T-1:Y6-BO film has a smoother surface with 1.53 nm roughness compared with 1.71 nm of the PBTFO-T-2:Y6-BO film. These results suggest that the PBTFO-T-1:Y6-BO film exhibits a better morphology with desirable roughness and phase separation for the higher J_{SC} and FF.

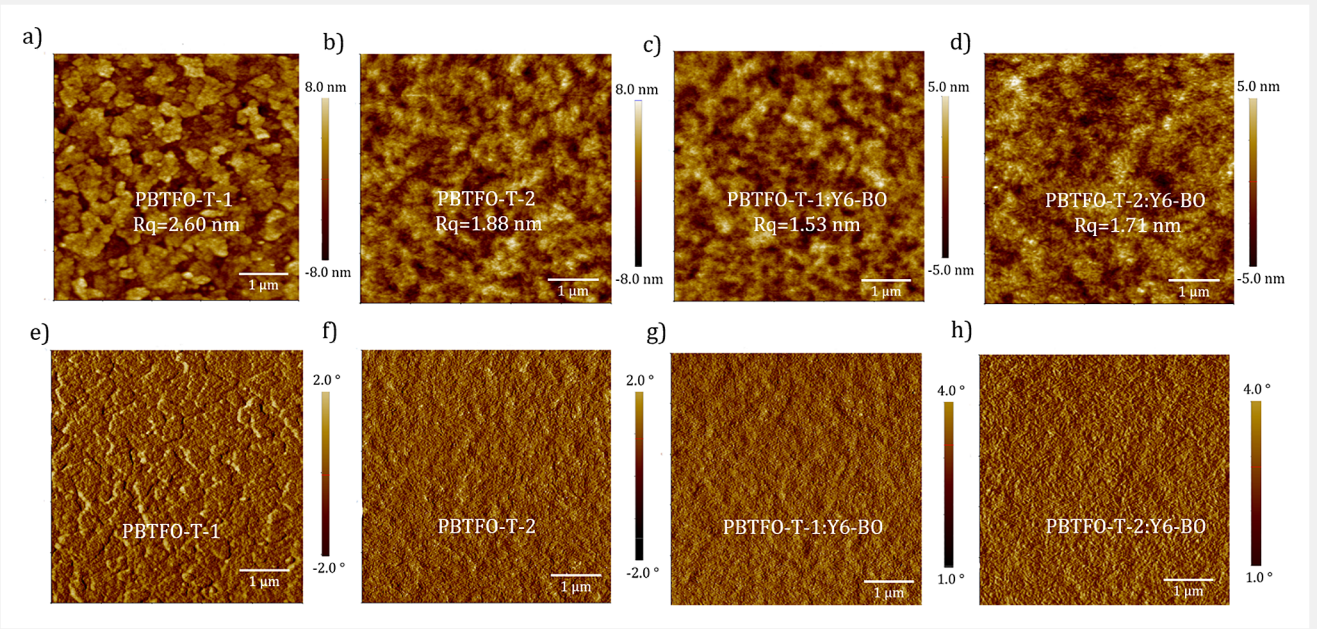

Figure 4 The AFM (5 μm × 5 μm) images of films.

Conclusions

In summary, a cost-effective copolymer PBTFO-T-1 has been designed and facilely synthesized via a straightforward three-step synthesis process. Another copolymer PBTFO-T-2 with regio-regularly oriented side chains was prepared to systematically investigate the influence of side chain orientation on polymer optoelectronic properties and photovoltaic performance of their corresponding PSCs. A considerable PCE of 14.16% can be achieved for PBTFO-T-1:Y6-BO-based devices via processing with the non-halogenated solvent o-xylene, which is significantly higher than 9.39% of the PBTFO-T-2:Y6-BO-based devices. It was demonstrated that PBTFO-T-1 exhibits more intense and ordered π–π stacking behavior than PBTFO-T-2, affording the higher J_{SC} and FF of the PBTFO-T-1:Y6-BO-based device due to the more balanced charge transfer ability, stronger exciton generation and dissociation, less carrier recombination and better morphology. This study provides a successful molecular design choice for developing polymer donors with low cost, green solvent processability as well as high performance for promoting the commercial application of PSC technology.

Experimental Section

General Materials and Methods

Compound **1** and other reagents used in the experiments were purchased from commercial sources such as Bidepharm, Energy Chemistry, and Jkchemical, and were used directly without further purification.

^{1}H NMR and ^{13}C NMR were recorded on a Bruker AVANCE 500 NMR spectrometer with tetramethylsilane as the internal reference. UV-vis absorption spectra were recorded on a Shimadzu UV-3600 spectrophotometer. Cyclic voltammetry measurements were carried out on a CHI660A electrochemical workstation at a scan rate of 100 mV·s^{-1} by using a platinum electrode as the counter electrode, Ag/AgCl electrode as the reference electrode, glassy carbon electrode as the working electrode, ferrocene as the internal standard and a 0.1 M solution of tetrabutylammonium hexafluorophosphate in acetonitrile as the electrolyte. AFM characteristics were carried out on a NanoMan VS microscope in the tapping mode. The molecular weights of the polymers were determined using a GPC 220 high-temperature chromatography system in 1,2,4-trichlorobenzene at 150 °C. TGA measurements were performed on a NETZSCH (DSC200F3) apparatus under a nitrogen atmosphere at a heating rate of 20 °C·min^{-1}. DSC measurements were performed on a NETZSCH (DSC200F3) apparatus under a nitrogen atmosphere with a heating/cooling rate of 10 °C·min^{-1} for both cycles. High-resolution mass spectra were measured by a Waters ACQUITY TQD mass spectrometer.

PSCs were fabricated with a conventional structure of ITO/PEDOT:PSS/active layer/NDI/Ag. The *J*–*V* curves were measured on a computer-controlled Keithley 2400 source meter under 1 sun (AM 1.5 G spectra) from a class solar simulator (Enlitech, Taiwan), and the light intensity was 100 m W/cm^2 as calibrated by a China General Certification Center-certified reference monocrystal silicon cell (Enlitech). The EQE spectra were recorded on a commercial EQE measurement system (Enlitech, Taiwan, QE-R3011).

The hole and electron mobilities of the devices were measured by the SCLC method. The structure of hole-only device was ITO/PEDOT:PSS/active layer/MoO_3/Ag, and it was ITO/ZnO/active layer/NDI/Ag for the electron-only device. The mobility was determined by fitting the dark current to the model of a single-carrier SCLC, which was described by the equation: $J = (9/8)\varepsilon_0\varepsilon_r\mu((V^2)/(d^3))$, where J is current density, μ is the zero-field mobility, ε_0 is the permittivity of the free space, ε_r is the relative permittivity of the material, d is the thickness of the active layers, and V is the effective voltage, which was obtained by subtracting the built-in voltage (V_{bi}) and the voltage drop (V_s) from the series resistance of the whole device except for the active layer from the applied voltage (V_{appl}), $V = V_{appl} - V_{bi} - V_s$. The mobility could be calculated from the slope of the $J^{1/2}$–V curves.

Synthetic Procedures of Intermediates and Polymers

4,7-Dibromo-5,6-difluorobenzo[*c*][1,2,5]thiadiazole (**2**):

Under an argon atmosphere, compound **1** (3.12 g, 18.0 mmol) was dissolved with 100 mL of concentrated sulfuric acid in a two-necked flask and protected from light and stirred well. Then 19.44 g (108.0 mmol) of NBS was added and the reaction was slowly heated to 60 °C for 4 h. After the reaction was completed, the reaction solution was cooled to room temperature and poured into the prepared ice water. The precipitate was obtained via filtration through a sand core funnel and washed repeatedly with deionized water for 3 times. Subsequently, the obtained solid was dissolved in dichloromethane and washed 3 times with saturated brine. The organic phase was dried with anhydrous magnesium sulfate, filtered and the filtrate was concentrated via rotary evaporation and then purified by silica gel column chromatography to afford compound **2** with a yield of 60%.

^{13}C NMR (126 MHz, $CDCl_3$): δ 152.95, 152.78, 150.87, 150.70, 148.87, 148.84, 99.47, 99.40, 99.35, 99.28.

HR-MS: Calcd. for $C_6Br_2F_2N_2S$: 329.9, Found: 330.1.

4,7-Dibromo-5-fluoro-6-((2-hexyldecyl)oxy)benzo[*c*][1,2,5]thiadiazole (**M1**):

Under an argon atmosphere, 2-hexyl-1-decanol (1.03 g, 4.2 mmol) was added to 40 mL of anhydrous tetrahydrofuran, followed by the addition of 60% sodium hydride (0.073 g, 3 mmol). The reaction mixture was stirred at 50 °C

for 3 h. After that, compound **2** (1.0 g, 3.03 mmol) was added and reacted overnight. After the reaction was completed, it was cooled to room temperature and transferred to a separatory funnel, which was washed with deionized water, dried with anhydrous magnesium sulfate, filtered, concentrated via rotary evaporation, and separated by silica gel column chromatography to obtain compound **M1** with a yield of 72%.

^{1}H NMR (500 MHz, $CDCl_3$): δ 4.13 (d, 2 H), 1.89–1.79 (m, 1 H), 1.59 (m, 2 H), 1.48–1.22 (m, 22 H), 0.89 (m, 6 H).

^{13}C NMR (126 MHz, $CDCl_3$): δ 157.72, 155.65, 150.01, 149.60, 149.45, 149.07, 149.02, 105.92, 105.89, 98.66, 98.48, 78.13, 78.09, 39.11, 31.97, 31.91, 31.87, 31.01, 31.00, 29.98, 29.66, 29.60, 29.34, 26.88, 26.84, 26.82, 22.74, 22.70, 22.68, 14.17, 14.13, 14.12.

HR-MS: Calcd. for $C_{22}H_{33}Br_2FN_2OS$: 552.4, Found: 553.4.

5-Fluoro-6-((2-hexyldecyl)oxy)benzo[*c*][1,2,5]thiadiazole (**3**):

Compound **1** (2 g, 11.62 nmol) and 2-hexyl-1-decanol (14.1 g, 58 mmol) were added to 100 mL of anhydrous tetrahydrofuran under an argon atmosphere. After the mixture was stirred homogeneously, potassium *tert*-butoxide (1.4343 g, 12.78 mmol) was added and stirred at 60 °C for 12 h. After the reaction, it was cooled to room temperature and transferred to a separatory funnel. It was extracted with ether, and the collected organic phase was dried with anhydrous magnesium sulfate. Then organic phase was filtrated and concentrated via rotary evaporation and separated by silica gel column chromatography to obtain compound **3** with a yield of 80%.

^{1}H NMR (500 MHz, $CDCl_3$): δ 7.57 (d, 1 H), 7.26 (d, 1 H), 4.00 (d, 2 H), 1.92 (m, 1 H), 1.39–1.21 (m, 24 H), 0.88 (m, 6 H).

^{13}C NMR (126 MHz, $CDCl_3$): δ 156.83, 154.76, 151.43, 151.04, 150.91, 148.69, 148.59, 103.66, 103.49, 98.72, 98.70, 71.32, 36.59, 30.87, 30.79, 30.28, 30.26, 28.92, 28.59, 28.53, 28.28, 25.77, 25.75, 21.65, 21.63, 13.08, 13.08.

HR-MS: Calcd. for $C_{22}H_{35}FN_2OS$: 394.6, Found: 395.6.

4-Bromo-6-fluoro-5-((2-hexyldecyl)oxy)benzo[*c*][1,2,5]thiadiazole (**4**):

Compound **3** (2.96 g, 7.49 nmol) was added to a mixed solution of 180 mL of dichloromethane and 90 mL of acetic acid under argon. After stirring well in the dark, Br_2 (9.6 g, 60 mmol) was added dropwise. The reaction was stirred for 48 h. After the reaction, it was transferred to a separatory funnel and extracted with dichloromethane. The combined organic phase was washed with deionized water, aqueous sodium bicarbonate solution and aqueous sodium sulfite solution in sequence. The collected organic phase was dried with anhydrous magnesium sulfate, filtered, concentrated via rotary evaporation, and separated by silica gel column chromatography to give compound **4** in 88% yield.

^{1}H NMR (500 MHz, $CDCl_3$): δ 7.63 (d, 1 H), 4.12 (d, 2 H), 1.84 (m, 1 H), 1.65–1.57 (m, 2 H), 1.39–1.20 (m, 22 H), 0.89 (d, J = 4.6 Hz, 6 H).

^{13}C NMR (126 MHz, $CDCl_3$): δ 160.06, 157.99, 151.33, 149.80, 149.70, 149.36, 149.21, 106.52, 106.48, 104.67, 104.49, 77.71, 77.68, 39.13, 31.91, 31.88, 31.04, 31.03, 30.00, 29.67, 29.61, 29.34, 26.85, 26.82, 22.70, 22.68, 14.13, 14.12.

HR-MS: Calcd. for $C_{22}H_{34}BrFN_2OS$: 473.5, Found: 474.4.

2,5-Bis(6-fluoro-5-((2-hexyldecyl)oxy)benzo[*c*][1,2,5]thiadiazol-4-yl)thiophene (**5**):

Compound **4** (2 g, 4.224 nmol) and 2,5-bis(trimethylstannyl)thiophene (0.8654 g, 2.1120 nmol) were added to a 150 mL two-necked flask. After three times of pumping and ventilation, $Pd(PPh_3)_4$ was added to it under argon, and 80 mL dry toluene was added. After the reaction solution was fully stirred, it was heated to 110 °C and stirred for 30 h. After the reaction, it was transferred to a separatory funnel and extracted with dichloromethane. The combined organic phase was washed with deionized water. The collected organic phase was dried with anhydrous magnesium sulfate, filtered, concentrated via rotary evaporation, and separated by silica gel column chromatography to obtain compound **5** in 50% yield.

^{1}H NMR (500 MHz, $CDCl_3$): δ 8.49 (s, 1 H), 7.61 (d, 1 H), 4.03 (d, 2 H), 1.97 (m, 1 H), 1.34–1.09 (m, 24 H), 0.85–0.75 (m, 6 H).

^{13}C NMR (126 MHz, $CDCl_3$): δ 160.51, 158.47, 151.23, 151.12, 150.72, 146.97, 146.83, 135.80, 135.77, 130.80, 119.16, 119.13, 103.94, 103.76, 77.86, 77.82, 39.07, 31.87, 30.99, 30.07, 29.74, 29.63, 29.33, 26.78, 26.74, 22.66, 22.64, 14.09, 14.04, 1.03.

HR-MS: Calcd. for $C_{48}H_{70}F_2N_4O_2S_3$: 869.3, Found: 868.6.

2,5-Bis(7-bromo-6-fluoro-5-((2-hexyldecyl)oxy)benzo[*c*][1,2,5]thiadiazol-4-yl)thiophene (**M2**):

Under argon, compound **5** (1.1 g, 1.265 mmol), 0.176 mL of Br_2 and $FeCl_3$ (4.1 mg, 0.0253 mmol) were added to a 150 mL two-necked flask, and 60 mL of chloroform was added as a solvent, and the reaction mixture was fully refluxed under stirring for 5 h. After the reaction, it was extracted with dichloromethane and washed with deionized water. The collected organic phase was dried with anhydrous magnesium sulfate, filtered, concentrated via rotary evaporation, and separated by silica gel column chromatography to obtain compound **M2** in 56% yield.

^{1}H NMR (500 MHz, $CDCl_3$): δ 8.47 (s, 1 H), 4.04 (d, 2 H), 1.98 (m, 1 H), 1.58–1.49 (m, 2 H), 1.45–1.36 (m, 2 H), 1.30–1.10 (m, 20 H), 0.82 (m, 6 H).

^{13}C NMR (126 MHz, $CDCl_3$): δ 158.18, 156.15, 150.37, 150.32, 149.41, 147.18, 147.04, 135.60, 135.57, 131.12, 118.40, 118.38, 97.43, 97.25, 78.34, 78.30, 39.06, 31.89, 31.87, 30.96, 30.94, 30.07, 29.73, 29.63, 29.34, 26.76, 26.74, 22.67, 22.65, 14.11, 14.05.

HR-MS: Calcd. for $C_{48}H_{68}Br_2F_2N_4O_2S_3$: 1027.1, Found: 1026.7.

Polymer PBTFO-T-1:

2,5-Bis(trimethylstannyl)thiophene (0.1 mmol), **M1** (0.1 mmol), tris(*o*-methylphenyl) phosphorus (0.016 mmol, 4.86 mg) and $Pd_2(dba)_3$ (0.002 mmol, 1.83 mg) were added to a 15 mL pressure tube under a nitrogen atmosphere. The mixture was dissolved in 1.8 mL toluene and 0.2 mL DMF, and then stirred at 120 °C for 24 h. After the mixture was cooled to room temperature, the product was precipitated in methanol and filtered. Then the precipitate was purified by Soxhlet extraction with acetone, hexane, dichloromethane and chloroform in sequence. The chloroform fraction was collected and concentrated, which was then precipitated into methanol and then filtered. The solid precipitate was dried under vacuum for 48 h to remove the solvent. The polymer was finally obtained as a blue solid in 76% yield.

GPC (1,2,4-trichlorobenzene, 150 °C, narrow standard): M_n = 38.0 kDa, PDI = 2.24.

Polymer PBTFO-T-2:

The preparation process of polymer PBTFO-T-2 is the same as that of PBTFO-T-1. The polymer was finally obtained as a blue solid in 81% yield.

GPC (1,2,4-trichlorobenzene, 150 °C, narrow standard): M_n = 34.6 kDa, PDI = 1.98.

Funding Information

This work was financially supported by the National Key Research and Development Program of China (No. 2019YFA0705900) funded by MOST, the National Natural Science Foundation of China (No. U21A6002) and the Basic and Applied Basic Research Major Program of Guangdong Province (No. 2019B030302007).

Supporting Information

Supporting Information for this article is available online at https://doi.org/10.1055/a-1833-8668.

Conflict of Interest

The authors declare no conflict of interest.

References

(1) Sun, Y.; Liu, T.; Kan, Y.; Gao, K.; Tang, B.; Li, Y. *Small Sci.* **2021**, *1*, 2100001.
(2) Li, G.; Zhu, R.; Yang, Y. *Nat. Photonics* **2012**, *6*, 153.
(3) Song, S.; Lee, K. T.; Koh, C. W.; Shin, H.; Gao, M.; Woo, H. Y.; Vak, D.; Kim, J. Y. *Energy Environ. Sci.* **2018**, *11*, 3248.
(4) Li, Y.; Huang, X.; Ding, K.; Sheriff, H. K. M., Jr.; Ye, L.; Liu, H.; Li, C. Z.; Ade, H.; Forrest, S. R. *Nat. Commun.* **2021**, *12*, 5419.
(5) Qin, L.; Liu, X.; Zhang, X.; Yu, J.; Yang, L.; Zhao, F.; Huang, M.; Wang, K.; Wu, X.; Li, Y.; Chen, H.; Wang, K.; Xia, J.; Lu, X.; Gao, F.; Yi, Y.; Huang, H. *Angew. Chem. Int. Ed.* **2020**, *59*, 15043.
(6) Xu, Y.; Yao, H.; Hou, J. *Chin. J. Chem.* **2019**, *37*, 207.
(7) Tang, C. W. *Appl. Phys. Lett.* **1986**, *48*, 183.
(8) Yu, G.; Gao, J.; Hummelen, J. C.; Wudl, F.; Heeger, A. J. *Science* **1995**, *270*, 1789.
(9) Søndergaard, R.; Hösel, M.; Angmo, D.; Larsen-Olsen, T. T.; Krebs, F. C. *Mater. Today* **2012**, *15*, 36.
(10) Fan, B.; Zhang, D.; Li, M.; Zhong, W.; Zeng, Z.; Ying, L.; Huang, F.; Cao, Y. *Sci. China Chem.* **2019**, *62*, 746.
(11) Cui, Y.; Yao, H.; Hong, L.; Zhang, T.; Xu, Y.; Xian, K.; Gao, B.; Qin, J.; Zhang, J.; Wei, Z.; Hou, J. *Adv. Mater.* **2019**, *31*, 1808356.
(12) Liu, Q.; Jiang, Y.; Jin, K.; Qin, J.; Xu, J.; Li, W.; Xiong, J.; Liu, J.; Xiao, Z.; Sun, K.; Yang, S.; Zhang, X.; Ding, L. *Sci. Bull.* **2020**, *65*, 272.
(13) Cui, Y.; Yao, H.; Hong, L.; Zhang, T.; Tang, Y.; Lin, B.; Xian, K.; Gao, B.; An, C.; Bi, P.; Ma, W.; Hou, J. *Natl. Sci. Rev.* **2020**, *7*, 1239.
(14) Huang, F.; Cao, Y. *Acta Polym. Sin.* **2016**, *4*, 399.
(15) Chen, S.; Feng, L.; Jia, T.; Jing, J.; Hu, Z.; Zhang, K.; Huang, F. *Sci. China Chem.* **2021**, *64*, 1192.
(16) Dai, S.; Zhan, X. *Acta Polym. Sin.* **2017**, *11*, 1706.
(17) Yuan, J.; Zhang, Y.; Zhou, L.; Zhang, G.; Yip, H.-L.; Lau, T.-K.; Lu, X.; Zhu, C.; Peng, H.; Johnson, P. A.; Leclerc, M.; Cao, Y.; Ulanski, J.; Li, Y.; Zou, Y. *Joule* **2019**, *3*, 1140.
(18) Luo, Z.; Liu, T.; Wang, Y.; Zhang, G.; Sun, R.; Chen, Z.; Zhong, C.; Wu, J.; Chen, Y.; Zhang, M.; Zou, Y.; Ma, W.; Yan, H.; Min, J.; Li, Y.; Yang, C. *Adv. Energy Mater.* **2019**, *9*, 1900041.
(19) Gao, K.; Kan, Y.; Chen, X.; Liu, F.; Kan, B.; Nian, L.; Wan, X.; Chen, Y.; Peng, X.; Russell, T. P.; Cao, Y.; Jen, A. K. *Adv. Mater.* **2020**, *32*, 1906129.
(20) Zhang, Y.; Cai, G.; Li, Y.; Zhang, Z.; Li, T.; Zuo, X.; Lu, X.; Lin, Y. *Adv. Mater.* **2021**, *33*, 2008134.
(21) Zhu, X.; Liu, S.; Yue, Q.; Liu, W.; Sun, S.; Xu, S. *CCS Chem.* **2021**, *3*, 1070.
(22) Lin, Y.; Zhao, F.; He, Q.; Huo, L.; Wu, Y.; Parker, T. C.; Ma, W.; Sun, Y.; Wang, C.; Zhu, D.; Heeger, A. J.; Marder, S. R.; Zhan, X. *J. Am. Chem. Soc.* **2016**, *138*, 4955.
(23) Ma, S.; Feng, H.; Liu, X.; Hu, Z.; Yang, X.; Liang, Y.; Zhang, J.; Huang, F.; Cao, Y. *ChemSusChem* **2021**, *14*, 3544.
(24) Zhang, Y.; Wang, Y.; Xie, Z.; Shan, T.; Zhu, L.; Liu, F.; Zhong, H. *J. Mater. Chem. C* **2020**, *8*, 17229.
(25) Cui, C.; Li, Y. *Energy Environ. Sci.* **2019**, *12*, 3225.
(26) Zhang, M.; Zhu, L.; Zhou, G.; Hao, T.; Qiu, C.; Zhao, Z.; Hu, Q.; Larson, B. W.; Zhu, H.; Ma, Z.; Tang, Z.; Feng, W.; Zhang, Y.; Russell, T. P.; Liu, F. *Nat. Commun.* **2021**, *12*, 309.
(27) Li, S.; Ye, L.; Zhao, W.; Yan, H.; Yang, B.; Liu, D.; Li, W.; Ade, H.; Hou, J. *J. Am. Chem. Soc.* **2018**, *140*, 7159.
(28) Yao, H.; Cui, Y.; Qian, D.; Ponseca, C. S., Jr.; Honarfar, A.; Xu, Y.; Xin, J.; Chen, Z.; Hong, L.; Gao, B.; Yu, R.; Zu, Y.; Ma, W.; Chabera, P.; Pullerits, T.; Yartsev, A.; Gao, F.; Hou, J. *J. Am. Chem. Soc.* **2019**, *141*, 7743.
(29) Zhao, W.; Qian, D.; Zhang, S.; Li, S.; Inganas, O.; Gao, F.; Hou, J. *Adv. Mater.* **2016**, *28*, 4734.

(30) Ren, J.; Bi, P.; Zhang, J.; Liu, J.; Wang, J.; Xu, Y.; Wei, Z.; Zhang, S.; Hou, J. *Natl. Sci. Rev.* **2021**, *8*, nwab031.
(31) Bin, H.; Gao, L.; Zhang, Z. G.; Yang, Y.; Zhang, Y.; Zhang, C.; Chen, S.; Xue, L.; Yang, C.; Xiao, M.; Li, Y. *Nat. Commun.* **2016**, *7*, 13651.
(32) Lan, L.; Chen, Z.; Hu, Q.; Ying, L.; Zhu, R.; Liu, F.; Russell, T. P.; Huang, F.; Cao, Y. *Adv. Sci.* **2016**, *3*, 1600032.
(33) Zheng, Z.; Hu, Q.; Zhang, S.; Zhang, D.; Wang, J.; Xie, S.; Wang, R.; Qin, Y.; Li, W.; Hong, L.; Liang, N.; Liu, F.; Zhang, Y.; Wei, Z.; Tang, Z.; Russell, T. P.; Hou, J.; Zhou, H. *Adv. Mater.* **2018**, *30*, 1801801.
(34) Osedach, T. P.; Andrew, T. L.; Bulović, V. *Energy Environ. Sci.* **2013**, *6*, 711.
(35) Yuan, D.; Pan, F.; Zhang, L.; Jiang, H.; Chen, M.; Tang, W.; Qin, G.; Cao, Y.; Chen, J. *Sol. RRL* **2020**, *4*, 2000062.
(36) Wang, Q.; Li, M.; Zhang, X.; Qin, Y.; Wang, J.; Zhang, J.; Hou, J.; Janssen, R. A. J.; Geng, Y. *Macromolecules* **2019**, *52*, 4464.
(37) Brabec, C. J.; Distler, A.; Du, X.; Egelhaaf, H. J.; Hauch, J.; Heumueller, T.; Li, N. *Adv. Energy Mater.* **2020**, *10*, 2001864.
(38) Pang, S.; Wang, Z.; Yuan, X.; Pan, L.; Deng, W.; Tang, H.; Wu, H.; Chen, S.; Duan, C.; Huang, F.; Cao, Y. *Angew. Chem. Int. Ed.* **2021**, *60*, 8813.
(39) Baran, D.; Ashraf, R. S.; Hanifi, D. A.; Abdelsamie, M.; Gasparini, N.; Rohr, J. A.; Holliday, S.; Wadsworth, A.; Lockett, S.; Neophytou, M.; Emmott, C. J.; Nelson, J.; Brabec, C. J.; Amassian, A.; Salleo, A.; Kirchartz, T.; Durrant, J. R.; McCulloch, I. *Nat. Mater.* **2017**, *16*, 363.
(40) Xiao, J.; Jia, X.; Duan, C.; Huang, F.; Yip, H. L.; Cao, Y. *Adv. Mater.* **2021**, *33*, 2008158.
(41) Yang, C.; Zhang, S.; Ren, J.; Gao, M.; Bi, P.; Ye, L.; Hou, J. *Energy Environ. Sci.* **2020**, *13*, 2864.
(42) Liu, F.; Zhang, J.; Zhou, Z.; Zhang, J.; Wei, Z.; Zhu, X. *J. Mater. Chem. A* **2017**, *5*, 16573.
(43) Sun, C.; Pan, F.; Bin, H.; Zhang, J.; Xue, L.; Qiu, B.; Wei, Z.; Zhang, Z.-G.; Li, Y. *Nat. Commun.* **2018**, *9*, 743.
(44) Wang, H.; Lu, H.; Chen, Y. N.; Ran, G.; Zhang, A.; Li, D.; Yu, N.; Zhang, Z.; Liu, Y.; Xu, X.; Zhang, W.; Bao, Q.; Tang, Z.; Bo, Z. *Adv. Mater.* **2021**, *34*, 2105483.
(45) Zhang, B.; Yu, Y.; Zhou, J.; Wang, Z.; Tang, H.; Xie, S.; Xie, Z.; Hu, L.; Yip, H. L.; Ye, L.; Ade, H.; Liu, Z.; He, Z.; Duan, C.; Huang, F.; Cao, Y. *Adv. Energy Mater.* **2020**, *10*, 1904247.
(46) Che, X.; Li, Y.; Qu, Y.; Forrest, S. R. *Nat. Energy* **2018**, *3*, 422.
(47) Chen, Y.; Cui, Y.; Zhang, S.; Hou, J. *Polym. Chem.* **2015**, *6*, 4089.
(48) Chen, X.; Liu, X.; Burgers, M. A.; Huang, Y.; Bazan, G. C. *Angew. Chem. Int. Ed.* **2014**, *53*, 14378.
(49) Mei, J.; Bao, Z. *Chem. Mater.* **2013**, *26*, 604.
(50) Burgués-Ceballos, I.; Machui, F.; Min, J.; Ameri, T.; Voigt, M. M.; Luponosov, Y. N.; Ponomarenko, S. A.; Lacharmoise, P. D.; Campoy-Quiles, M.; Brabec, C. J. *Adv. Funct. Mater.* **2014**, *24*, 1449.
(51) McDowell, C.; Bazan, G. C. *Curr. Opin. Green Sustainable Chem.* **2017**, *5*, 49.
(52) Chen, S. H.; Liao, C. H.; Chang, C. Y.; Huang, K. M.; Chen, J. Y.; Chen, C. H.; Meng, H. F.; Zan, H. W.; Horng, S. F.; Lin, Y. C.; Yeh, M. H. *Org. Electron.* **2019**, *75*, 105376.
(53) Zhang, Q.; Kelly, M. A.; Bauer, N.; You, W. *Acc. Chem. Res.* **2017**, *50*, 2401.
(54) Hong, L.; Yao, H.; Wu, Z.; Cui, Y.; Zhang, T.; Xu, Y.; Yu, R.; Liao, Q.; Gao, B.; Xian, K.; Woo, H. Y.; Ge, Z.; Hou, J. *Adv. Mater.* **2019**, *31*, 1903441.
(55) He, D.; Zhao, F.; Wang, C.; Lin, Y. *Adv. Funct. Mater.* **2022**, 2111855.
(56) Mihailetchi, V. D.; Koster, L. J.; Hummelen, J. C.; Blom, P. W. *Phys. Rev. Lett.* **2004**, *93*, 216601.
(57) Zhang, X.; Jiang, D.-W.; Yang, G.-L.; Zhu, Y.-C.; Tian, J.; Cao, H.-L.; Gao, Y.; Zhang, W.-A. *Chin. J. Polym. Sci.* **2021**, *39*, 692.
(58) Tang, H.; Chen, H.; Yan, C.; Huang, J.; Fong, P. W. K.; Lv, J.; Hu, D.; Singh, R.; Kumar, M.; Xiao, Z.; Kan, Z.; Lu, S.; Li, G. *Adv. Energy Mater.* **2020**, *10*, 2001076.
(59) Mihailetchi, V. D.; Wildeman, J.; Blom, P. W. *Phys. Rev. Lett.* **2005**, *94*, 126602.
(60) Koster, L. J. A.; Mihailetchi, V. D.; Xie, H.; Blom, P. W. M. *Appl. Phys. Lett.* **2005**, *87*, 203502.
(61) Wetzelaer, G. A. H.; Kuik, M.; Lenes, M.; Blom, P. W. M. *Appl. Phys. Lett.* **2011**, *99*, 153506.